Genome-wide CRISPR screens identify novel regulators of wild-type and mutant p53 stability

YiQing Lü[1, 2], Tiffany Cho[1,2], Saptaparna Mukherjee[3], Ahmad Malik[1,2], Nicolas S. Gonzalez-Foutel[4], Robin Oh[1], Ellen Langille[1, 2], Khalid N. Al-Zahrani[1], Zhen Yuan Lin[1], Varda Rotter[3], Patricia Ashton-Prolla[5], Lucia B. Chemes[4], Jason Moffat[2,6], Anne-Claude Gingras[1,2], Moshe Oren[3], Daniel Durocher[1,2] and Daniel Schramek[1,2 *]

[1] Centre for Molecular and Systems Biology, Lunenfeld-Tanenbaum Research Institute, Mount Sinai Hospital, Toronto, Ontario, Canada

[2] Department of Molecular Genetics, University of Toronto, Toronto, Ontario, Canada

[3] Department of Molecular Cell Biology, Weizmann Institute of Science, Rehovot, Israel

[4] Instituto de Investigaciones Biotecnológicas (IIBiO-CONICET), Universidad Nacional de San Martín, Buenos Aires, Argentina

[5] Departamento de Genética, UFRGS and Serviço de Genetica Médica HCPA, Porto Alegre, Brasil

[6] Donnelley Centre, Toronto, Ontario, Canada.

* Correspondence and requests for materials should be addressed to Daniel Schramek

Daniel Schramek, PhD
Lunenfeld-Tanenbaum Research Institute
Mount Sinai Hospital
Toronto, Ontario, Canada M5G 1X5
Phone: +1 416 586-4800
Fax: +1 416 586-8869
schramek@lunenfeld.ca

Abstract

Tumour suppressor p53 (*TP53*) is the most frequently mutated gene in cancer. Several hotspot p53 mutants not only lose tumour suppressive capabilities, but also function in a dominant-negative manner, suppressing canonical wild-type p53 function. Furthermore, some hotspot p53 mutants promote oncogenesis by gain-of-function mechanisms. Levels of p53 are regulated predominantly through regulation of protein stability and while wild-type p53 is normally kept at very low levels at steady-state, p53 mutants are often stabilized in tumours, which may be vital for their oncogenic properties. Here, we systematically profiled the factors that regulate protein stability of wild-type and mutant p53 using marker-based genome-wide CRISPR screens. We found that most proteins that regulate wild-type p53 also regulate a subset of p53 mutants with the exception of p53 R337H regulators, which are largely private to this mutant. Mechanistically, we identified FBXO42 as novel positive regulator of a subset of mutant p53 comprising R273H, R248Q and R248W. We show that, FBXO42 acts together with CCDC6 to regulate USP28-mediated p53 stabilization. Our work also identifies C16orf72 as negative regulator of wild-type p53 stability as well as stability of all p53 mutants tested. *C16orf72* is amplified in breast cancer, and we show that C16orf72 regulates p53 levels in mammary epithelium of mice and its overexpression can drive breast cancer formation. Together, this work provides a network view of the process that regulates p53 stability, which might provide clues for targeting of wild-type or mutant p53 in cancer.

Introduction

Approximately half of all tumours harbor mutations in the p53 (*TP53*) gene, making *TP53* the most commonly mutated gene in cancer[1-4]. The majority of these mutations are missense mutations, most of which not only deprive p53 of its tumor suppressor activities, but might also function in a dominant-negative manner suppressing the canonical p53 function upon oligomerization with wild-type p53[5-9]. Some missense mutations also confer a so-called gain-of-functions (GOF) phenotype, converting mutant p53 into a cancer-promoting protein that renders cancer cells more malignant by increasing growth rate, motility, invasion, drug resistance and tumorigenicity, while reducing apoptotic rate[1, 3, 10-17]. Importantly, compared to tumors with wild-type p53 or those lacking p53 altogether, tumors expressing GOF mutant p53 are more invasive, metastatic, and proliferative, and display increased genome instability and chemoresistance in mouse and man[3, 12, 18-23]. Two main classes of p53 hotspot mutations have been distinguished – those that affect residues directly involved in protein-DNA interaction, such as R248 or R273 ('contact mutants'), and those that affect residues involved in stabilizing the tertiary structure of the protein, such as R175, G245, R249 and R282 ('conformational' or 'structural' mutants).

Germline *TP53* mutations also exist, often target the same hotspot residues, and are the underlying cause of Li-Fraumeni Syndrome, which predisposes to a wide spectrum of early-onset cancers. In Brazil, the *TP53* R337H founder mutation exists in high frequency and represents the most common germline *TP53* mutation reported to date[24]. Interestingly, this mutation is not located in the DNA binding domain of p53, like most hotspot mutations, but in the oligomerization domain and disrupts p53 oligomerization.

While wild-type p53 protein is maintained at very low levels, mutant p53 is often stabilized and highly overexpressed in tumors, which is thought to be required for mutant p53 to exert its oncogenic effects. In fact, strong immunohistochemical staining patterns of nuclear p53 still serve as a surrogate marker for *TP53* mutations in the clinic[25, 26]. Interestingly, knock-in mouse models of p53 and Li-Fraumeni patients carrying germline p53 GOF mutations highly express mutant p53 specifically in tumor cells, but show low or undetectable levels of mutant p53 in the surrounding, phenotypically normal tissues[3, 18, 19, 27]. This observation indicates that mutant p53 is not intrinsically stable and that its levels are kept in check in healthy cells, but that this regulation is perturbed in cancer[3, 18, 19]. The stability of wild-type p53 is regulated mainly through MDM2/4-mediated ubiquitination and degradation[28-30] but little is known about the factors that regulate mutant p53 stability.

Here, we employed functional genomics and proteomics approaches to systematically profile the processes that regulate the stability of wild-type and of the most common p53 mutants that collectively account for ~50% of all mutant p53[24]. These screens identified 864 genes whose loss either increases or

decreases stability of p53 mutants. Mining this dataset, we report that the FBXO42-CCDC6-USP28 axis acts as a positive regulator of mutant p53 stability and C16orf72-HUWE1-USP7 axis acts as a negative regulator of p53 stability.

Results

A fluorescence-based p53 stability reporter system

To monitor p53 stability at the single-cell level, we generated a lentiviral protein stability reporter (**Fig 1a**) consisting of a p53-mClover-P2A-mRFP cassette that permits translation of a mClover-p53 protein fusion and a red fluorescent RFP protein from the same mRNA transcript, similar to previous protein stability reporters[31, 32]. The co-translational self-cleaving P2A peptide generates a p53-mClover fusion protein to assess p53 stability, while mRFP serves as an internal control to monitor expression of the bicistronic transgene. Any perturbation that results in overall increased transcription or general differences of proteostasis would affect mRFP as well as p53-mClover, while any perturbation that specifically affects p53 stability would result in an altered mClover/mRFP ratio (**Fig. 1a**).

To benchmark this reporter, we used an hTERT-immortalized retinal pigment epithelium-1 (RPE1) cell line that expresses Cas9 and was previously used in CRISPR screens[33]. We used a RPE1 subclone in which the gene encoding p53 was knocked out by gene editing[34] and generated isogenic lines expressing stability reporters containing either wild-type p53 or 8 of the most common hotspot p53 mutations (R175H, G245S, R248Q, R248W, R249S, R273H, R282W, and R337H). As a control, we also generated a cell line expressing the mClover-P2A-RFP cassette. We observed that cells transduced with p53 G245S, R248Q, R248W or R273H exhibited bimodal distribution of p53 levels, with one subset expressing hardly any p53 and the other subset expressing higher levels of p53. This pattern of p53 protein expression was observed with both structural (G245S) and contact (R248Q, R248W, R273H) p53 mutants (**Fig. 1b**). Such bimodal distribution was observed in lymphoma cell lines expressing endogenous p53 R248Q, R248W or R273H mutants [35] and thus likely reflects the intrinsically unstable nature of mutant p53[27]. In line with previous data showing that MDM2 promotes the degradation of wild-type and some mutant p53[27, 29, 36], treatment with the MDM2 inhibitor Nutlin-3a elevated the levels of wild-type p53 and the p53 mutants G245S, R248Q, R248W, and R273H, while p53 R175H, R249S, R282W and R337H did not respond to Nutlin-3a (**Fig 1b**). Upon removal of Nutlin-3a, levels of wild-type p53 and mutant p53 returned to baseline levels re-establishing the uni- or bimodal distribution of the starting population (**Fig. 1b**). Similarly, we observed that irradiation led to significantly increased levels of p53 mutants (G245S, R248Q, R248W, R273H) with the exception of p53 R175H, R249S, R282W, and R337H (**Suppl. Fig. 1a**), further indicating that most p53 mutants are regulated by the same machinery that regulates wild-type p53. In line with these data,

CRISPR/Cas9-mediated ablation of MDM2 elevated the $p53^{R273H}$-mClover, which could be reversed by ectopically re-expressing MDM2, further validating our reporter system (**Fig. 1c**).

Genome-wide CRISPR screens identifies regulators of wild-type and mutant p53 stability

To identify regulators of p53 stability, we performed genome-wide pooled CRISPR screens in RPE1-hTERT Cas9 cells expressing either the control mClover-P2A-RFP cassette or the stability reporters for p53 wild-type, R175H, G245S, R248Q, R273H, or R337H. We used the TKOv3 lentiviral sgRNA library, which contains 70,948 guides (~4 guides/gene) targeting 18,053 protein-coding genes and 142 control sgRNAs targeting EGFP, LacZ and luciferase[37]. We transduced the reporter lines at 200X coverage, selected for infected cells and isolated cell populations expressing low or high p53-mClover by flow cytometry (**Fig. 1d**). For reporter lines with a unimodal p53 distribution, we sorted cells with the lowest and highest 15% of p53-mClover expression, and for lines with a bimodal p53 distribution, we isolated the lower and the upper populations. sgRNA abundance of the initial sgRNA plasmid library, the input cells after transduction (T0) and the sorted samples were quantified using deep sequencing to identify enriched and depleted sgRNAs. The 7 cell lines were screened in duplicates at a minimum and we observed a high reproducibility between replicates (r = 0.44 - 0.71)[33] (**Suppl. Fig. 1b**).

For gene-level depletion/enrichment, we calculated a normalized z-score of the low and high p53-mClover populations combining multiple sgRNAs per gene. Negative NormZ scores represent genes whose mutation leads to decreased p53 levels (i.e. positive regulators of p53 stability), whereas positive NormZ scores represent genes whose mutation leads to increased p53 levels (i.e. negative regulators of p53 stability). As expected, sgRNAs targeting p53 and mClover were the most depleted sgRNAs, while sgRNAs targeting MDM2 or MDM4 were among the most enriched sgRNAs in the p53-high populations. Other known positive regulators of p53 such as ATM, USP28, TTI1/2, TP53BP1, or CHEK2 and negative regulators of p53 stability such as USP7, HUWE1 or PPM1D/G also scored in several p53 wild-type or mutant screens, further validating the screens (**Fig. 1e and f** and **Suppl. Fig. 2a-d**). Unsupervised clustering of the screens showed that p53 wild-type, G245S, R248Q, R273H mutants clustered closely together, while R175H p53 and p53 R337H showed distinct profiles (**Fig. 1g**).

To identify hits, we selected genes with a NormZ values +/- 3 and a false discovery rate (FDR) lower than 0.5 and excluded genes that also affected the empty control mClover-P2A-mRFP reporter. These cutoffs identified 317 and 547 genes, whose loss led to decreased and increased p53 levels, respectively. While most genes regulated stability of wild-type and several p53 mutants, we also identified p53 wild-type- and p53 mutant-specific regulators (**Fig. 1h**). For example, wild-type p53 levels were specifically sensitive to perturbation of the 20S and 19S proteasomal subunits, consistent with the high protein turn-over of p53. This is in contrast to the levels of some mutant p53, such as R273H and R248Q, whose level were not significantly affected upon genetic ablation of proteasome subunits (**Suppl. Fig. 2e**). In addition, of the 317 hits whose loss caused p53 destabilization, the vast majority (183 genes) regulated only p53 R337H.

Conversely, of the 547 hits whose loss led to p53 stabilization, only a small subset (52 genes) regulated p53 R337H (**Fig. 1h, Suppl. Fig. 1B**). These data suggest that p53 R337H is controlled by mechanisms that are different from those modulating wild-type p53 and all other p53 mutants tested.

FBXO42-CCDC6 axis regulates wild-type and mutant p53 stability

One of the strongest hits in the R273H and R248Q screen was *FBXO42* (NormZ value of -4.05 for R273H and -5.65 for R248Q), coding for F-Box Protein 42, which functions as substrate-recognition part of an SCF (SKP1-CUL1-F-box protein)-type E3 ubiquitin ligase complex. Analysis of the Dependency Map (DepMap) project indicated that the genetic dependency profile of *FBXO42* correlated with that of p53 and its activators *CHEK2*, *TP53BP1*, *ATM* and *USP28* and was inversely correlated with those of negative p53 regulators such as *MDM2*, *MDM4*, *PPM1G* and *USP7* (**Fig 2a, b**), strongly suggesting a functional connection to the p53 pathway. The strongest genetic co-dependency of *FBXO42* and one of the strongest correlations across all genes and cell lines, is with *CCDC6*, which encodes a coiled-coil domain containing protein (**Fig. 2a** and **b**). CCDC6 shows a similarly strong co-dependency with the p53 pathway in DepMap and loss of *CCDC6* caused phenotypes nearly identical to those associated with the loss of *FBXO42* in our screens, i.e. resulting in decreased p53 R273H and R248Q levels (**Fig. 2c** and **Suppl. Table 1**).

To validate these findings, we used two independent sgRNAs with good on-target efficacy to confirm the effect of FBXO42 and CCDC6 loss on p53 stability and used sgRNAs targeting the *AAVS1* locus as control (**Suppl. Fig. 2f**). We observed significantly reduced R273H, R248Q and R248W p53mClover levels but failed to see an effect on wild-type, R175H, G245S or R337H p53-mClover levels (**Fig. 2d** and **Suppl. Fig. 3a**), indicating specificity between p53 mutations. The difference in p53 levels was even more apparent upon irradiation (**Suppl. Fig. 3b-d**) and in single cell knock-out clones (**Fig. 2e**). We also tested whether proteasomal degradation is involved in FBXO42/CCDC6-mediated regulation of mutant p53. Inhibition of the proteasome by MG132 significantly increased mutant p53 levels in FBXO42 and CCDC6 knock-out cells as assessed by WB analysis and flow cytometry whereas it had little impact in *AAVS1*-targeted cells (**Fig. 2e** and **Suppl. Fig. 3e**). Importantly, genetic ablation of *FBXO42* also reduced levels of p53 in the pancreatic cancer cell lines PANC-1 which is homozygous for p53 R273H[38] (**Fig. 2f**), without affecting *TP53* mRNA expression, indicating that FBXO42 may act on p53 via posttranscriptional regulation (**Suppl. Fig. 3f**).

To test for a potential epistatic relationship between FBXO42 and CCDC6, we used isogenic *FBXO42*-knockout (Δ*FBXO42*), *CCDC6*-knockout (Δ*CCDC6*) and *AAVS1*-targeted control RPE-1 $p53^{R273H}$-mClover reporter cell lines (**Fig. 2e**). As expected, $p53^{R273H}$-mClover levels in Δ*FBXO42* and Δ*CCDC6* could be partially rescued by re-expressing FBXO42 or CCDC6, respectively. While expression of FBXO42 did not rescue $p53^{R273H}$-mClover levels in Δ*CCDC6* cells, we found that expression of CCDC6 partly rescued mutant p53 levels in $FBXO42^{KO}$ cells (**Fig. 2g**), suggesting that FBXO42 may function upstream of CCDC6.

Using FBXO42 truncation mutants, we found that both the Kelch and F-Box domains are required to promote $p53^{R273H}$ stabilization, indicating that FBXO42's ability to stabilize $p53^{R273H}$ is dependent on substrate binding by its Kelch domains and F-Box mediated assembly of an SCF complex with SKP1 and CUL1, likely to promote SKP1/CUL1-mediated ubiquitination (**Fig. 2h** and **Suppl. Fig. 3g, h**). Together, these data indicate that FBXO42 and CCDC6 function as positive post-translational regulators of wild-type p53 and several p53 mutants in a ubiquitination-dependent manner.

Mapping of the FBXO42-CCDC6 and mutant p53 interaction network

To investigate how FBXO42-CCDC6 regulates p53 stability, we identified vicinal proteins by proximity-dependent biotinylation coupled to mass spectrometry (BioID)[39-42] using inducible expression of biotin ligase (BirA*)-tagged FBXO42, CCDC6 or $p53^{R273H}$ in HEK293 Flp-In T-REx cells. Given that proteasome-dependent nature of this regulatory circuit, we performed these BioID experiments in the absence or presence of MG132. The resulting mass spectrometry data were thresholded for minimum spectral count and fold change over control as well as filtered via significance analysis of interactome (SAINT)[43], which uses a probability model to assign a confidence score to each interaction and compared to a large dataset of 192 BioID experiments (CRAPome)[44]. Consistent with its role as an SCF-E3 ligase, the top interactors for FBXO42 were CUL1 and SKP1. FBXO42 BioID also enriched for CCDC6, p53 itself as well as several proteins known to regulate p53 such as HUWE1 or BRCA2 (**Fig. 3a**). $p53^{R273H}$ proximal proteins included known p53 interactors such as MDM2, BRCA2, HUWE1, USP28, TP53BP1, PPM1G, BLM, ATRX and PML (**Fig. 3a**). In addition, endogenous CCDC6 co-immunoprecipitated (co-IP) with endogenous p53 R273H and the reciprocal co-IP also showed that endogenous mutant p53 interacted with V5-tagged CCDC6 in PANC1 cells (**Fig. 3b** and **Suppl. Fig. 4a**). In further support of this interaction, proximity ligation assay (PLA) showed that CCDC6 and $p53^{R273H}$ interact with each other in the nucleus and the cytoplasm (**Fig. 3c**). Using *in vitro* binding assays of recombinant proteins, we detected a direct interaction between FBXO42 Kelch domains 1-3 and the core DNA-binding domain of p53 R273H (**Fig. 3d, Supp Fig. 3h**), further supporting the results of the domain-mutant rescue experiments and the enzymatic role of this E3 ubiquitin ligase. Together, these data indicate that R273H p53 interacts with both its regulators CCDC6 and FBXO42. Since the latter also interact (BioID), this suggests a higher order complex may be formed that regulates p53 stability.

FBXO42-CCDC6 regulates p53 via USP28

To identify genetic determinants of FBXO42/CCDC6-mediated $p53^{R273H}$ stabilization, we performed secondary genome-wide CRISPR screens using isogenic Δ*FBXO42*, Δ*CCDC6* or control RPE1 $p53^{R273H}$-mClover-P2A-RFP reporter cell lines. This allowed us to systematically map genetic perturbation that regulate $p53^{R273H}$ stability depending on the presence of FBXO42 and CCDC6 (**Fig. 3e and f**). Most genes such as *MDM2*, *MDM4*, *USP7*, *CSNK1A1*, *ATM* or *TTI* retained their function in regulating p53 stability in

Δ*FBXO42* or Δ*CCDC6* RPE1 cells. As expected for genes in the same pathway and based on our previous data, *CCDC6* did not score in the Δ*FBXO42* screen (nor did *FBXO42)* and *FBXO42* did not score in the Δ*CCDC6* screen (nor did *CCDC6)*. Interestingly, we identified one F-Box protein coding-gene, *FBXL18*, which gained the ability to reduce $p53^{R273H}$-mClover levels in Δ*FBXO42* or Δ*CCDC6* RPE1 cells but did not have an effect when lost in parental RPE1 wild-type cells, suggesting that FBXL18 may compensate for the loss of FBXO42/CCDC6 (**Fig. 3e and f**). In addition, loss of *USP28*, whose perturbation led to the strongest reduction in $p53^{R273H}$-mClover levels in the wild-type RPE1, had no effect on $p53^{R273H}$-mClover levels in the screen in Δ*FBXO42* cells, and only a weak effect on $p53^{R273H}$-mClover levels in Δ*CCDC6* RPE1 cells, indicating that USP28 may function in the same pathway as FBXO42/CCDC6 (**Fig. 3e and f**). We could corroborate these genetic interactions and show that concomitant loss of *USP28* has no effect on $p53^{R273H}$-mClover levels in Δ*FBXO42* or Δ*CCDC6* RPE1 cells (**Suppl. Fig. 4b**). Loss of *FBXO42* or *CCDC6* resulted in decreased levels of nuclear USP28 as shown by nuclear/cytoplasmic fractionation as well as immunofluorescence (**Fig. 3g** and **Suppl. Fig. 4c**). Importantly, ectopic expression of either FBXO42 or CCDC6 not only rescued the USP28 levels in Δ*FBXO42* or Δ*CCDC6* RPE1 cells but also led to increased USP28 levels in "wild-type" RPE1 cells concomitant with a slight upregulation of p53 levels (**Fig. 3h**). Genetic ablation of *FBXO42* or *CCDC6* in PANC1 cells also reduced USP28 protein levels without affecting USP28 transcript levels (**Fig. 3i** and **Suppl. Fig. 4d**), indicating that the post-translational regulation of USP28 by FBXO42/CCDC6 is not unique to RPE1 cells. Next, we generated Δ*USP28* $p53^{R273H}$-mClover RPE1 cells and assessed how overexpression of FBXO42 and CCDC6 impacted $p53^{R273H}$ levels (**Suppl. Fig. 4e**). While expressing USP28 rescued $p53^{R273H}$ levels, overexpressing FBXO42 or CCDC6 in Δ*USP28* cells had no effect, indicating that the FBXO42/CCDC6 act via USP28. Moreover, we found that USP28 overexpression rescue mutant p53 levels in Δ*FBXO42* or Δ*CCDC6* RPE1 cells, indicating that USP28 is downstream of FBXO42/CCDC6 (**Suppl. Fig. 4e**). Together, these data indicate that FBXO42/CCDC6 control mutant p53 levels via USP28.

Synthetic viability screen maps positive regulators of p53

Our results support the notion that the molecular machinery and physiological stress triggers that regulate wild-type p53 stability also regulates mutant p53, except for $p53^{R337H}$. This is also exemplified by our screens, which identified many more genes whose loss leads to p53 stabilization compared to genes whose loss leads to reduced p53 levels. To better understand the set of genes whose loss leads to p53 stabilization, we performed pathway analysis using gProfiler (**Fig. 4a**). Gene sets associated with cell cycle, mitotic anaphase, cellular response to stress, extracellular stimuli or hypoxia, separation of sister chromatids, stabilization of p53 and p53-dependent and -independent DNA Damage Responses were highly significantly enriched. Enrichment was also found for genes involved in regulation of SLITs and ROBOs and nonsense-mediated decay. Interestingly, metabolism of RNA and rRNA processing in the nucleus and

cytosol were the most significantly enriched categories. This functional group was also enriched in various other screens to identify genes that cause genomic instability, modulate responses to ionizing or UV radiation or for ATM/ATR substrates[45-48], indicating that RNA metabolism is tightly interconnected with DNA damage Responses. Together, this data indicates that stability of mutant p53 is to a large extent regulated by the physiological machinery that regulates stress-induced wild-type p53 stability. However, this data also indicates that most of the hits whose loss leads to p53 stabilization might regulate p53 in a rather indirect manner by triggering a stress response.

As an alternative approach to identify regulators of p53, we sought to exploit the concept of synthetic viability, which describes a genetic interaction where viability of one genetic mutation is determined by the presence of second genetic mutation[49]. The mutations in *MDM2* and *TP53* display a synthetic viability interaction as the embryonic and cellular lethality associated with the loss of MDM2 is completely rescued in a p53 null background[50]. To identify the full repertoire of genes that are synthetic viable with p53, we performed genome-wide CRISPR screens in isogenic p53-proficient and -deficient RPE1 cell lines where data was analyzed with BAGEL2[51] where positive Bayes factors (BF) values identify genes that are likely essential for proliferation. Synthetic viable interactions were defined as genes that had high BF values in p53-proficient cells but negative values in the p53-deficient cell line. As expected, the known negative p53 regulators MDM2, MDM4, USP7, PPM1D (encoding WIP1) all scored highly as synthetic viability hits in the screen. In addition, pathway analysis of the top 150 scoring genes using PANTHER[52] revealed enrichment genes involved in p53 pathways (p53 pathway feedback loop 1 and 2, p-value < 0.01) and a related pathway (Ubiquitin proteasome pathway, p-value < 0.01) (**Fig. 4c**).

To delineate high confidence p53 regulators, we looked for hits that scored in both the p53 synthetic viable and the p53 reporter screens. 11 out of the 20 top-scoring genes in the synthetic viability screen also scored in the p53 reporter screen with *C16orf72* as top hit. In addition to the well-known p53 regulators (*MDM2/4, USP7, PPM1D*), *ZNF574, APEX2, CSNK1A, BRAP, NONO, PPP2CA* and *TCOF1* also scored prominently in both screening paradigms (**Fig. 4d;** and **Suppl. Table 2**).

C16orf72 (also known as *TAPR1*) was previously identified in a screen for genes that altered sensitivity to telomere attrition and was shown to buffer against p53 activation in response to telomer erosion [53] and we recently identified C16orf72 in a screen that analyzed genetic vulnerabilities to ATR inhibition[54]. In addition, analysis of coessentiality across 789 cancer cell lines from the DepMap project showed a striking association between *C16orf72* and several positive and negative p53 regulators (**Fig. 4e** and **f)**[53, 55]. Together, these data identified C16orf72 as a candidate negative regulator of p53 stability.

C16orf72 is a regulator of wild-type and mutant p53 stability

To validate the genetic interaction between *TP53* and *C16orf72*, we performed clonogenic survival assays. Loss of *C16orf72* resulted in decreased cell viability and relative cellular fitness selectively in the $TP53^{+/+}$ background but had no impact in the p53-deficient isogenic counterpart, indicating synthetic viability (**Fig. 5a** Loss of *C16orf72* also caused an increased in p53 levels for both wild-type as well as all tested p53 mutants (**Fig. 5b, c** and **Suppl. Fig. 5a**).

To gain further insight into the putative functions of C16orf72, we performed immunoprecipitation coupled to mass spectrometry (IP-MS) on FLAG-tagged C16orf72. This identified HUWE1 as a prominent interactor of C16orf72, in line with previous findings[53]. HUWE1 is a known E3 ubiquitin ligase for p53, scored as a hit in our marker-based p53 stability screens and showed strongest co-essentiality in DepMap (**Fig. 2C and 4g)**. However, we did not identify HUWE1 as a hit in our synthetic viability screen and siRNA mediated knock-down of HUWE1 only led to a moderate increase in p53 levels compared to loss of other known negative p53 regulators such as MDM2 or USP7 (**Fig. 5d**). Together, these data indicate that there might be mechanisms other than HUWE1 involved in the stabilization of p53 following *C16orf72* loss or that the p53-depenedent modulation of p53 is complex, masking its potential role alongside C16orf72 in that cell line.

The second most significant co-essential gene of *C16orf72* in DepMap was *USP7* (**Fig. 4f and g**), which also scored as synthetic viable p53 interaction as well as a strong p53 stability regulator in our CRISPR screens (**Fig. 2c** and **4b**). To test a potential functional relationship between C16orf72 and USP7, we performed co-immunoprecipitation experiments and found that FLAG-tagged full-length USP7 can interact with HA-tagged C16orf72 (**Fig. 5e**). Together, this indicates that C16orf72 might regulate p53 via USP7.

C16orf72 functions as oncogene and regulates p53 stability in the mammary gland

Strikingly, the *USP7* gene lies directly adjacent to *C16orf72* and both genes are commonly co-amplified in up to 8% of cancer as well as being co-gained in up to 53% of cases ($p<0.001$; **Suppl. Fig. 5b** and **c**). Invasive breast cancer showed the highest level of amplification (7.5%) and gains (28%) of the *USP7*/*C16orf72* locus ($p<0.001$; **Suppl. Fig. 5d**). These two co-amplified negative p53 regulators might therefore cooperate in modulating p53 levels in cancer.

To test the role of *C16orf72 in vivo*, we first conducted multicolour competition assays in the of LSL-Cas9-GFP mice. Intraductal injection of lentiviral particles expressing Cre, RFP and a sgRNA cassette targeting *Mdm2* or *C16orf72* led to a drastic reduction of mammary epithelial cells of LSL-Cas9-GFP mice when compared to a control lentivirus expressing Cre, BFP and an sgRNA targeting the inert Tigre locus. The reduced cell viability was dependent on p53 as conditional p53 knock-out mice (*Trp53*$^{fl/fl}$; LSL-Cas9-GFP) did not show an overt phenotype (**Fig. 6a**).

Conversely, overexpression of *C16orf72* led to significant reduction in p53^{R273} levels in RPE1 cells (**Fig. 6b**) and levels of wild-type p53 expression human *Pik3ca*^{H1047R}-mutant mammary epithelial MCF10A (**Fig. 6c**). This led us to hypothesize whether overexpression of *C16orf72* can decrease latency of *Pik3ca*^{H1047R}-driven mammary tumors. Of note, loss of p53 cooperates with *Pik3ca*^{H1047R} to accelerate mammary tumor initiation (**Suppl. Fig. 5e**) [56, 57]. Like loss of p53 or overexpression of Mdm2 as our positive control, intraductal injection of lentiviral particles expressing a Cre and *C16orf72* expression cassette into LSL-*Pik3ca*^{H1047R} mice significantly reduced latency of *Pik3ca*^{H1047R}-driven mammary tumor development compared to vector only Cre-lentivirus (**Fig. 6d**). Interestingly, we did not observe any synergistic effect of combined *C16orf72* with *Usp7* expression on *Pik3ca*^{H1047R}-driven mammary tumor development (**Fig. 5d**).

Discussion

Over 22 million cancer patients today carry *TP53* mutations, the majority of which are missense mutations, often resulting in elevated expression of mutant p53 proteins[2]. Lowering mutant p53 expression can reduce tumor growth and metastasis and trigger tumor regression[58-60], suggesting that tumors become addicted to mutant p53. Targeting factors that regulate mutant p53 stability or reactivate wild-type p53 function might therefore constitute a viable therapeutic strategy.

We therefore conducted genome-wide CRISPR screens in isogenic RPE1 cells expressing protein stability reporters for wild-type p53 and five of the most common p53 mutants. Unsupervised hierarchical clustering showed that most hotspot mutant p53 proteins (R175H, G245S, R248Q, R273H) are regulated by a common molecular network, which is to a certain degree distinct from wild-type p53. Interestingly, the Brazilian founder mutation R337H, which is located in the oligomerization domain and the only mutation outside of the DNA binding domain, behaved drastically different to the other hotspot mutations and wild-type p53. As such, it will be interesting to further elucidate the molecular underpinnings why some mutations behave like wild-type p53, while others do not. Together, these data provide a comprehensive map of genes that regulate wildtype and mutant p53 protein stability and might have implications for the development of agents that target mutant p53 in cancer therapy.

We next characterized two mutant p53 regulators FBXO42 and CCDC6 and provided strong genetic evidence that FXBO42 in conjunction with CCDC6 are novel regulators of certain mutant p53. FBXO42 was previously reported as a negative regulator of wild-type p53 and shown to bind a phosphodegron on p53 leading to its proteasomal degradation in U2OS cells[61]. The COP9 signalosome-associated kinase mediated phosphorylation of p53's core DNA binding domain, which was required to allow FBXO42 binding and ubiquitination[62]. We found no significant effect of FBXO42 on wild-type p53

or R175H, G245S or R337H p53, but genetic ablation of FBXO42 caused destabilization of p53 R273H, R248Q and R248W, showing that FBXO42 functions as positive regulator of mutant p53 protein levels in RPE1 and PANC1 cells. This is consistent with the co-dependencies of FBXO42 and CCDC6 in DepMap, which clearly align them with positive p53 regulators such as ATM, CHEK2, TP53BP1 and USP28 and anticorrelated with negative p53 regulators such as MDM2/4, TTC1 or PPM1G/D. This discrepancy might be due to the cell line, p53 status and culture conditions. Interestingly, other previously reported regulators mutant p53 stability such as TRRAP, BAG2 or BAG5 did not score as hits in our screen, suggesting that context may be important for p53 regulation[35, 63-65].

Similarly, we found that CCDC6 also regulates the same p53 mutants and CCDC6 and FBXO42 were recently shown to interact genetically[66, 67]. We corroborated this interaction data and show that they also interact physically. In addition, we found an interaction between CCDC6 and p53 (by PLA and IP) and a direct interaction between FBXO42's Kelch domains and R273H p53. Epistasis experiments showed that FBXO42 appears to function upstream of CCDC6 in regulating p53. In addition, we also found that another well -known p53 regulator, BRCA2, is interacting with mutant p53 and also surfaced as FBXO42 vicinal protein and potential FBXO42 target (Fig. 3a). However, it is still unclear whether these interactions are required to regulate p53 protein levels and the exact mechanism remains elusive.

Using further genetic screening in FBXO42- and CCDC6-knockout R273H p53 reporter query lines and additional epistasis experiments, we uncovered a genetic interaction of FBXO42/CCDC6 with USP28. USP28 was originally implicated as a protective deubiquitinating enzyme counteracting the proteasomal degradation of p53, TP53BP1, CHCK2, and additional proteins[68-71]. USP28 regulates wild-type p53 via TP53BP1-dependent and -independent mechanisms. Concordantly, our data shows that USP28 and TP53BP1 are strong positive regulators of wild-type p53. However, while USP28 was also a strong hit in the mutant R273H p53 screen, TP53BP1 was not, indicating that the effects we see upon loss of USP28 on R273H p53 are independent of TP53BP1. In addition, we found that genetic ablation of FBXO42 or CCDC6 leads to a significant reduction of nuclear USP28 levels, adding further biochemical support to the genetic interaction data. While the exact molecular mechanisms are currently unclear, we provide strong evidence that FBXO42/CCDC6 is required for USP28-mediated regulation of R273H p53 stability, indicating that interfering with this regulatory circuit could present an avenue to prevent or reduce mutant p53 accumulation in tumors.

USP28 also regulates other important proteins such as MYC by counteracting FBXW7-mediated proteasomal degradation as well as cJun, Notch1, LSD1, HIF-1a and MDC1[71]. It will be interesting to elucidate whether FBXO42 and CCDC6 also impinge on those cellular pathways or whether there is some selectivity.

Our data also shows that there are many genes whose loss results in increased p53 levels, which presumably is rooted in the fact that any gene loss which causes cellular stress will probably indirectly lead to p53 stabilization. Therefore, we cross-referenced our p53 stability screen with a synthetic viable screen, which revealed a key role of C16orf72 as a negative regulator of wild-type and mutant p53. The role of C16orf72 in p53 regulatory mechanism is further supported by the mutual exclusivity of *TP53* genetic alteration and *C16orf72* amplification, which is observed 8% of breast cancer genomes from the METABRIC study ($p < 0.001$). However, the direct implication on the role of *C16orf72* amplification towards tumor development is complicated by the fact that *USP7* gene is located adjacent to C16orf72 locus, resulting in concurrent amplification of *USP7* and C16orf72. In addition, recurrent *de novo* copy number alterations encompassing *USP7* and *C16orf72* are also seen in autism spectrum disorder[72], and the role of p53 and the DNA damage response pathway in neurodegenerative diseases and autism is increasingly recognized[73, 74], further indicating a potentially interesting connection.

By generating autochthonous breast cancer mouse models, we could show that overexpression of *C16orf72* or *USP7* independently accelerates *Pik3ca*^{H1047R}-driven mammary tumor formation. Mechanistically, we show that C16orf72 interacts with USP7 and HUWE1, which are *bone fide* regulators of p53 potentially hinting at how C16orf72 may regulate p53 stability. Our findings are also in line with a recent report showing that C16orf72 is crucial in mediating telomere attrition-induced p53-dependent apoptosis and in regulating the effects of ATR inhibition[53, 54].

In summary, our study provides a rich resource to mine for candidate regulators of wild-type and mutant p53 stability, provides a template to reveal regulators of any protein of interest on a genome-wide level and identified several positive (FBXO42 and CCDC6) as well as negative (C16orf72) regulators of p53 stability.

Supplementary Information contains all Methods, Supplementary Fig. 1-5, Supplementary Fig. legends and Supplementary Tables 1&2.

Acknowledgements. We would like to thank all members of our laboratories as well as, Mikko Taipale, Brian Raught and The Centre for Phenogenomics (TCP) for helpful discussions. We want to thank Henrique Melo for assistance with data analysis, Annie Bang, Michael Parsons and Dione White in the Lunenfeld-Tanenbaum Research Institute Flow Cytometry Facilities for assistance with FACS, Kin Chan at the Lunenfeld Network Biology Centre for assistance with next generation sequencing, and Andrew Elia at the University Health Network for assistance with histology. Research in this work is supported by fundings from the Joint Canada-Israel Research Programme (D.S., M.O., V.R., AC.G., P.A.P., and L.B.C., CIHR IRDC 384428). D.D was supported by a grant from the Canadian Cancer Society (705644). Y.Q.L. is the recipient of doctoral fellowships from the Canadian Institute of Health Research (CIHR 157921 and MSFSS 431649), Government of Ontario (OGS) and the University of Toronto. D.S. is supported by the Canada Research Chair programme. P.A-P was supported by a scholarship from CNPq (Conselho Nacional de Desenvolvimento Científico e Tecnológico, Brazil, # 307826/2017-1).

Author Contributions. Y.L. performed all p53 stability screens and almost all FBXO42/CCDC6 and C16orf72 mouse experiments. T.C. performed the p53 synthetic viability screens and most of the biochemical C16orf72 experiments. S.M. helped performed CCDC6 IP and PLA experiments. A.M. helped with bioinformatics. R.O., E.L. and K.N.A. helped with mouse experiments. Z.Y.L. together with A.C.G. performed mass spectrometry. N.G.F. together with L.B.C. performed FBXO42-p53 binding experiments. V.R. and P.P helped with conceptualization of the project. J.M. helped with CRISPR screens. Y.L., T.C., DD, M.O. and D.S. designed the experiments and coordinated the project, and together with Y.L. and D.S. wrote the manuscript.

Competing interests. All authors declare no competing interests.

References

1. Vogelstein, B., Lane, D. & Levine, A.J. Surfing the p53 network. *Nature* **408**, 307-310 (2000).
2. Petitjean, A. *et al.* Impact of mutant p53 functional properties on TP53 mutation patterns and tumor phenotype: lessons from recent developments in the IARC TP53 database. *Hum Mutat* **28**, 622-629 (2007).
3. Oren, M. & Rotter, V. Mutant p53 gain-of-function in cancer. *Cold Spring Harb Perspect Biol* **2**, a001107 (2010).
4. Freed-Pastor, W.A. & Prives, C. Mutant p53: one name, many proteins. *Genes Dev* **26**, 1268-1286 (2012).
5. Varley, J.M. *et al.* A detailed study of loss of heterozygosity on chromosome 17 in tumours from Li-Fraumeni patients carrying a mutation to the TP53 gene. *Oncogene* **14**, 865-871 (1997).
6. Malkin, D. Li-fraumeni syndrome. *Genes Cancer* **2**, 475-484 (2011).
7. Liu, D.P., Song, H. & Xu, Y. A common gain of function of p53 cancer mutants in inducing genetic instability. *Oncogene* **29**, 949-956 (2010).
8. Chene, P. In vitro analysis of the dominant negative effect of p53 mutants. *J Mol Biol* **281**, 205-209 (1998).
9. Giacomelli, A.O. *et al.* Mutational processes shape the landscape of TP53 mutations in human cancer. *Nat Genet* **50**, 1381-1387 (2018).
10. Weisz, L. *et al.* Transactivation of the EGR1 gene contributes to mutant p53 gain of function. *Cancer Res* **64**, 8318-8327 (2004).
11. Zalcenstein, A. *et al.* Mutant p53 gain of function: repression of CD95(Fas/APO-1) gene expression by tumor-associated p53 mutants. *Oncogene* **22**, 5667-5676 (2003).
12. Blandino, G., Levine, A.J. & Oren, M. Mutant p53 gain of function: differential effects of different p53 mutants on resistance of cultured cells to chemotherapy. *Oncogene* **18**, 477-485 (1999).
13. Peled, A., Zipori, D. & Rotter, V. Cooperation between p53-dependent and p53-independent apoptotic pathways in myeloid cells. *Cancer Res* **56**, 2148-2156 (1996).
14. Muller, P.A. & Vousden, K.H. p53 mutations in cancer. *Nat Cell Biol* **15**, 2-8 (2013).
15. Wolf, D., Harris, N. & Rotter, V. Reconstitution of p53 expression in a nonproducer Ab-MuLV-transformed cell line by transfection of a functional p53 gene. *Cell* **38**, 119-126 (1984).
16. Dittmer, D. *et al.* Gain of function mutations in p53. *Nat Genet* **4**, 42-46 (1993).
17. Eliyahu, D., Raz, A., Gruss, P., Givol, D. & Oren, M. PARTICIPATION OF P53 CELLULAR TUMOR-ANTIGEN IN TRANSFORMATION OF NORMAL EMBRYONIC-CELLS. *Nature* **312**, 646-649 (1984).
18. Olive, K.P. *et al.* Mutant p53 gain of function in two mouse models of Li-Fraumeni syndrome. *Cell* **119**, 847-860 (2004).
19. Lang, G.A. *et al.* Gain of function of a p53 hot spot mutation in a mouse model of Li-Fraumeni syndrome. *Cell* **119**, 861-872 (2004).
20. Liu, G. *et al.* High metastatic potential in mice inheriting a targeted p53 missense mutation. *Proc Natl Acad Sci U S A* **97**, 4174-4179 (2000).
21. Zerdoumi, Y. *et al.* Drastic effect of germline TP53 missense mutations in Li-Fraumeni patients. *Hum Mutat* **34**, 453-461 (2013).
22. Bougeard, G. *et al.* Molecular basis of the Li-Fraumeni syndrome: an update from the French LFS families. *J Med Genet* **45**, 535-538 (2008).
23. Morton, J.P. *et al.* Mutant p53 drives metastasis and overcomes growth arrest/senescence in pancreatic cancer. *Proc Natl Acad Sci U S A* **107**, 246-251 (2010).
24. Bouaoun, L. *et al.* TP53 Variations in Human Cancers: New Lessons from the IARC TP53 Database and Genomics Data. *Hum Mutat* **37**, 865-876 (2016).
25. Rotter, V. p53, a transformation-related cellular-encoded protein, can be used as a biochemical marker for the detection of primary mouse tumor cells. *Proc Natl Acad Sci U S A* **80**, 2613-2617 (1983).
26. Yemelyanova, A. *et al.* Immunohistochemical staining patterns of p53 can serve as a surrogate marker for TP53 mutations in ovarian carcinoma: an immunohistochemical and nucleotide sequencing analysis. *Mod Pathol* **24**, 1248-1253 (2011).
27. Terzian, T. *et al.* The inherent instability of mutant p53 is alleviated by Mdm2 or p16INK4a loss. *Genes Dev* **22**, 1337-1344 (2008).
28. Eischen, C.M. & Lozano, G. The Mdm network and its regulation of p53 activities: a rheostat of cancer risk. *Hum Mutat* **35**, 728-737 (2014).

29. Haupt, Y., Maya, R., Kazaz, A. & Oren, M. Mdm2 promotes the rapid degradation of p53. *Nature* **387**, 296-299 (1997).
30. Kubbutat, M.H., Jones, S.N. & Vousden, K.H. Regulation of p53 stability by Mdm2. *Nature* **387**, 299-303 (1997).
31. Yen, H.C., Xu, Q., Chou, D.M., Zhao, Z. & Elledge, S.J. Global protein stability profiling in mammalian cells. *Science* **322**, 918-923 (2008).
32. Yu, T. *et al.* Profiling human protein degradome delineates cellular responses to proteasomal inhibition and reveals a feedback mechanism in regulating proteasome homeostasis. *Cell Res* **24**, 1214-1230 (2014).
33. Hart, T. *et al.* High-Resolution CRISPR Screens Reveal Fitness Genes and Genotype-Specific Cancer Liabilities. *Cell* **163**, 1515-1526 (2015).
34. Noordermeer, S.M. *et al.* The shieldin complex mediates 53BP1-dependent DNA repair. *Nature* **560**, 117-121 (2018).
35. Jethwa, A. *et al.* TRRAP is essential for regulating the accumulation of mutant and wild-type p53 in lymphoma. *Blood* **131**, 2789-2802 (2018).
36. Lukashchuk, N. & Vousden, K.H. Ubiquitination and degradation of mutant p53. *Mol Cell Biol* **27**, 8284-8295 (2007).
37. Hart, T. *et al.* Evaluation and Design of Genome-Wide CRISPR/SpCas9 Knockout Screens. *G3 (Bethesda)* **7**, 2719-2727 (2017).
38. Redston, M.S. *et al.* p53 mutations in pancreatic carcinoma and evidence of common involvement of homocopolymer tracts in DNA microdeletions. *Cancer Res* **54**, 3025-3033 (1994).
39. Lambert, J.P., Tucholska, M., Go, C., Knight, J.D. & Gingras, A.C. Proximity biotinylation and affinity purification are complementary approaches for the interactome mapping of chromatin-associated protein complexes. *J Proteomics* **118**, 81-94 (2015).
40. Roux, K.J., Kim, D.I. & Burke, B. BioID: a screen for protein-protein interactions. *Curr Protoc Protein Sci* **74**, Unit 19 23 (2013).
41. Kim, D.I. *et al.* An improved smaller biotin ligase for BioID proximity labeling. *Mol Biol Cell* **27**, 1188-1196 (2016).
42. Roux, K.J., Kim, D.I., Raida, M. & Burke, B. A promiscuous biotin ligase fusion protein identifies proximal and interacting proteins in mammalian cells. *J Cell Biol* **196**, 801-810 (2012).
43. Teo, G. *et al.* SAINTq: Scoring protein-protein interactions in affinity purification - mass spectrometry experiments with fragment or peptide intensity data. *Proteomics* **16**, 2238-2245 (2016).
44. Mellacheruvu, D. *et al.* The CRAPome: a contaminant repository for affinity purification-mass spectrometry data. *Nat Methods* **10**, 730-736 (2013).
45. Paulsen, R.D. *et al.* A genome-wide siRNA screen reveals diverse cellular processes and pathways that mediate genome stability. *Mol Cell* **35**, 228-239 (2009).
46. Stokes, M.P. *et al.* Profiling of UV-induced ATM/ATR signaling pathways. *Proc Natl Acad Sci U S A* **104**, 19855-19860 (2007).
47. Hurov, K.E., Cotta-Ramusino, C. & Elledge, S.J. A genetic screen identifies the Triple T complex required for DNA damage signaling and ATM and ATR stability. *Genes Dev* **24**, 1939-1950 (2010).
48. Matsuoka, S., Huang, M. & Elledge, S.J. Linkage of ATM to cell cycle regulation by the Chk2 protein kinase. *Science* **282**, 1893-1897 (1998).
49. O'Neil, N.J., Bailey, M.L. & Hieter, P. Synthetic lethality and cancer. *Nat Rev Genet* **18**, 613-623 (2017).
50. Montes de Oca Luna, R., Wagner, D.S. & Lozano, G. Rescue of early embryonic lethality in mdm2-deficient mice by deletion of p53. *Nature* **378**, 203-206 (1995).
51. Kim, E. & Hart, T. Improved analysis of CRISPR fitness screens and reduced off-target effects with the BAGEL2 gene essentiality classifier. *Genome Med* **13**, 2 (2021).
52. Mi, H. *et al.* PANTHER version 11: expanded annotation data from Gene Ontology and Reactome pathways, and data analysis tool enhancements. *Nucleic Acids Res* **45**, D183-D189 (2017).
53. Benslimane, Y. *et al.* A novel p53 regulator, C16ORF72/TAPR1, buffers against telomerase inhibition. *Aging Cell* **20**, e13331 (2021).
54. Hustedt, N. *et al.* A consensus set of genetic vulnerabilities to ATR inhibition. *bioRxiv*, 574533 (2019).

55. Amici, D.R. *et al.* Coessential Genetic Networks Reveal the Organization and Constituents of a Dynamic Cellular Stress Response. *bioRxiv*, 847996 (2019).
56. Langille, E.R. *et al.* Loss of epigenetic regulation disrupts lineage integrity, reactivates multipotency and promotes breast cancer. *bioRxiv*, 2021.2010.2022.465428 (2021).
57. Adams, J.R. *et al.* Cooperation between Pik3ca and p53 mutations in mouse mammary tumor formation. *Cancer Research* **71**, 2706-2717 (2011).
58. Bossi, G. *et al.* Mutant p53 gain of function: reduction of tumor malignancy of human cancer cell lines through abrogation of mutant p53 expression. *Oncogene* **25**, 304-309 (2006).
59. Hui, L., Zheng, Y., Yan, Y., Bargonetti, J. & Foster, D.A. Mutant p53 in MDA-MB-231 breast cancer cells is stabilized by elevated phospholipase D activity and contributes to survival signals generated by phospholipase D. *Oncogene* **25**, 7305-7310 (2006).
60. Alexandrova, E.M. *et al.* Improving survival by exploiting tumour dependence on stabilized mutant p53 for treatment. *Nature* **523**, 352-356 (2015).
61. Sun, L. *et al.* JFK, a Kelch domain-containing F-box protein, links the SCF complex to p53 regulation. *Proc Natl Acad Sci U S A* **106**, 10195-10200 (2009).
62. Sun, L. *et al.* Substrate phosphorylation and feedback regulation in JFK-promoted p53 destabilization. *J Biol Chem* **286**, 4226-4235 (2011).
63. Yue, X. *et al.* BAG2 promotes tumorigenesis through enhancing mutant p53 protein levels and function. *Elife* **4** (2015).
64. Yue, X. *et al.* A novel mutant p53 binding partner BAG5 stabilizes mutant p53 and promotes mutant p53 GOFs in tumorigenesis. *Cell Discov* **2**, 16039 (2016).
65. Zhao, Y. *et al.* Pontin, a new mutant p53-binding protein, promotes gain-of-function of mutant p53. *Cell Death Differ* **22**, 1824-1836 (2015).
66. Shimada, K., Bachman, J.A., Muhlich, J.L. & Mitchison, T.J. shinyDepMap, a tool to identify targetable cancer genes and their functional connections from Cancer Dependency Map data. *Elife* **10** (2021).
67. Garofano, L. *et al.* Pathway-based classification of glioblastoma uncovers a mitochondrial subtype with therapeutic vulnerabilities. *Nat Cancer* **2**, 141-156 (2021).
68. Zhang, D., Zaugg, K., Mak, T.W. & Elledge, S.J. A role for the deubiquitinating enzyme USP28 in control of the DNA-damage response. *Cell* **126**, 529-542 (2006).
69. Cuella-Martin, R. *et al.* 53BP1 Integrates DNA Repair and p53-Dependent Cell Fate Decisions via Distinct Mechanisms. *Mol Cell* **64**, 51-64 (2016).
70. Lambrus, B.G. *et al.* A USP28-53BP1-p53-p21 signaling axis arrests growth after centrosome loss or prolonged mitosis. *J Cell Biol* **214**, 143-153 (2016).
71. Wang, X. *et al.* Targeting deubiquitinase USP28 for cancer therapy. *Cell Death Dis* **9**, 186 (2018).
72. Sanders, S.J. *et al.* Multiple recurrent de novo CNVs, including duplications of the 7q11.23 Williams syndrome region, are strongly associated with autism. *Neuron* **70**, 863-885 (2011).
73. Chang, J.R. *et al.* Role of p53 in neurodegenerative diseases. *Neurodegener Dis* **9**, 68-80 (2012).
74. Wong, S. *et al.* Role of p53, Mitochondrial DNA Deletions, and Paternal Age in Autism: A Case-Control Study. *Pediatrics* **137** (2016).
75. Zimmermann, M. *et al.* CRISPR screens identify genomic ribonucleotides as a source of PARP-trapping lesions. *Nature* **559**, 285-289 (2018).

Figure Legends

Figure 1. CRISPR screen for regulators of wild-type and mutant p53 stability

(A) Reporter design. Schematic of the fluorescence reporter based bicistronic p53 stability sensor. The bicistronic design separates changes in p53 levels due to gene expression (#1 diagonal axis) from post-translational modification (#2 horizontal axis) by assessing the intensities of the monomeric fluorophores in living cells using flow cytometry

(B) Flow cytometry blots depicting the level of wild-type and mutant p53 protein reporters upon MDM2-p53 inhibition using Nultin-3a (10 uM, 24 hours) and its withdrawal (24 hours).

(C) Flow cytometry blots depicting the level of wild-type and R273H p53 protein reporters upon CRISPR/Cas9-mediated MDM2 depletion or upon subsequent MDM2 overexpression measured 7 days post-transduction.

(D) Schematic of the screening set up and analysis. Each clonal reporter line was transduced with a lentiviral genome-wide CRISPR knockout library (TKOv3). Infected populations were drug selected and sorted by Fluorescence-Activated Cell Sorting (FACS) into mClover-low and mClover-high pools. sgRNA barcodes were amplified and their abundance in each pool was determined by next generation sequencing.

(E, F) Screen results for wild-type and R273H p53 protein reporters. Volcano plots displaying the perturbation effects (log 2-fold change, LFC) of each gene based on two replicates per screen. To compare among different screens (G, H), the perturbation effects of each gene was further normalised as normZ scores, considering both the LFC and FDR values. Hits were defined as having $|normZ| \geq 3$. On the volcano plots, hits satisfying both FDR > 0.5 and LFC $\geq$ 1 (red) or LFC $\leq$ -0.8 (blue) were labelled.

(G) Unsupervised hierarchy clustering of the wild-type and five screened p53 mutants, using the screening results based on all 18053 genes.

(H) UpSet plot displaying hits shared amongst each mutant screened. The loss-of-function of an “up” or “down” hit would result in that p53 mutant to destabilise or stabilise, respectively.

Figure 2. FBXO42-CCDC6 axis regulates mutant p53 protein stability

(A) Coessentiality heatmap of top genes correlated and anti-correlated with *FBXO42* in DepMap.

(B) The 50 top genes correlated (blue) and anti-correlated (red) with *FBXO*42 within 789 CIRPSR screens (depmap.org).

(C) Hierarchical clustering displaying the effects of selected hits whose genetic ablation alters protein stability in wild-type and five p53 mutants.

(D) Flow cytometry blots depicting the level of wild-type and R273H p53 protein reporters upon CRISPR/Cas9-mediated depletion of indicated genes. Independent sgRNAs different from the sgRNAs in the screening library were used (red) and the effects were compared against control guides targeting the AAVS1 safe harbour (blue).

(E) p53 protein levels in RPE1 R273H reporter cell line upon clonal depletion of *CCDC6* or *FBXO42*, and upon proteasomal inhibition (10 uM MG132 for 12 hours).

(F) Representative Western Blot results showing p53 protein levels in PANC1 cells upon depletion of *CCDC6* and *FBXO42*, and upon genotoxic stress (IR 0.5 Gy, 24 hours after). GAPDH serves as loading control. Bar graph depicts quantification of p53 levels over 3 independent experiments (*: $p<0.05$). Error bar = standard error of the mean (S.E.M.).

(G) Flow cytometry blots depicting the level of R273H p53 protein reporter upon depletion of *CCDC6* or *FBXO42* and re-expression of *CCDC6* or *FBXO42*.

(H) Flow cytometry blots depicting the level of R273H p53 protein reporter upon depletion of *FBXO42* and re-expression of indicated FBXO42 truncation mutants.

Figure 3. Mapping the genetic interaction network of FBXO42-CCDC6 and mutant p53.

(A) Putative interactors of R273H, CCDC6 and FBXO42 as mapped by BioID in HEK293-FlpIn lines stably expressing each bait, with or without the proteasomal inhibitor MG 132 [5 uM, 24 hours].

(B) Interaction of CCDC6 and p53R273H in PANC1 cells validated using immunoprecipitation (IP). Lysates of PANC1 cells with or without depletion of the endogenous $p53^{R273H}$ protein were immunoprecipitated using an CCDC6-specific antibody or an IgG-isotype control, followed by Western blot analysis of endogenous p53.

(C) Proximity ligation assay (PLA) between CCDC6 and $p53^{R273H}$ in PANC1 cells, with or without depletion of the endogenous $p53^{R273H}$ protein, using tetramethylrhodamine-5-isothiocyanate (TRITC) as a probe (red) and counterstained with DAPI (blue) and phalloidin-FITC (green) to visualise nuclear DNA and F-actin, respectively.

(D) *In vitro* binding assay of p53 core domain with the FBXO42 kelch domain. The MBP-tagged FBXO42-Kelch domain (FBXO42c), and the core DNA-binding domain of $p53^{R273H}$ (p53-CD-R273H, untagged) were expressed and purified from bacteria. Untagged p53-CD-R273H does not interact with Amylose resin, while MBP-FBXO42c is pulled down by Amylose. Upon incubation of MBP-FBXO42c and p53-CD-R273H, p53-CD-R273H was found in the pulled down fraction; the input, Amylose-bound and Amylose-unbound fractions were resolved in SDS-PAGE and stained with Coomassie Blue.

(E, F) Scatter plots of the perturbation effect of each gene as normalised Z-score (normZ), in the R273H reporters before and after the loss of *CCDC6* or *FBXO42*. Selected genes whose depletion resulted in p53 stabilisation and destabilisation are marked in red and green, respectively.

(G, H) Representative Western blot results showing levels of USP28 and p53 in nuclear and cytoplasmic fractions of the R273H reporter cell line with clonal depletion of FBXO42 or CCDC6, and upon the ectopic re-expression of CCDC6 or FBXO42. Histone H3 serves as a nuclear and GAPDH as a cytoplasmic markers.

(I) Total cellular USP28 and p53 levels in PANC1 cells upon depletions of *CCDC6*, *FBXO42*, or *USP28*.

Figure 4. Synthetic viability screen maps regulators of p53.

(A) Gene Ontology term enrichment analysis performed on genes whose loss leads to stabilization of wild-type p53. Genes with normZ score of >3.0 from the stability screen were used.

(B) Synthetic viability screen. Bayesian Factors (BF) as a measurement of essentiality (high values indicate a lethal gene) are blotted for all protein-coding genes in p53 wild-type versus p53 null background.

(C) Pathway analysis based on the top scoring genes in the synthetic viability screen using PANTHER pathway analysis, and pathway enrichments with p<0.01 are listed.

(D) Venn diagram showing the hits from the synthetic viability screen as well as the hits from the wildtype and R273H p53 stability screen.

(E) Coessentiality heatmap of top genes correlated and anti-correlated with *C16orf72* in DepMap.

(F) The top 50 genes correlated (blue) and anti-correlated (red) with *C16orf72*, based on results from genome-wide cell fitness screens performed in 789 cancer cell lines (depmap.org).

Figure 5. C16orf72 is a regulator of wild-type and mutant p53 stability.

(A) Vvalidation of synthetic viability by C16orf72 via clonogenic survival assays. The total of 200 puromycin-selected cells were plated and grown for 13 sgRNA-treated plate were computed from the plating efficiency and the number of colonies obtained in each plate (N=3).

(B) Representative Western Blot results showing p53 and p21 protein levels in RPE1 cells upon depletion of *C16orf72* and *MDM2*.

(C) Flow cytometry blots depicting the level of wild-type or R273H p53 protein in reporters upon depletion of *C16orf72*.

(D) Representative Western Blot results showing p53 protein levels in response to depletion of *C16orf72* and other known E3 ligases of p53 using siRNAs (*MDM2*, *USP7* and *HUWE1*).

(E) Interaction of C16orf72 and USP7 in RPE1 cells validated using co-immunoprecipitation (co-IP). Lysates of RPE1 cells overexpressing HA-tagged C16orf72 or a vector control construct with FLAG-tagged USP7 or its vector control, were co-IPed using a FLAG-specific antibody, followed by Western Blot analysis of HA (HA-C16orf72). The input materials are shown on the left.

Figure 6. C16orf72 functions as oncogene and regulates p53 stability in the mammary gland

(A) *In vivo* cell competition assay in the mammary gland. Blot shows percent of surviving cells transduced with the indicated sgRNA normalized to control.

(B) Flow cytometry blots depicting the level of R273H p53 protein reporter upon overexpression of *C16orf72*.

(C) Western blot analysis of wildtype p53 levels in human MCF10A mammary epithelial cells overexpressing C16orf72, assayed after treatment with Doxorubicin [2 μg/mL] for 6 hours.

(D) Kaplan-Meier plot depicting the tumour-free survival of tumour-prone mouse line ($Pi3k^{H1047R}$) overexpressing C16orf72, Usp7, Mdm2, C16orf72+Usp7, or control (mRuby), delivered via mammary ductal injection of lentiviruses carrying each ORF. (n=5 for each condition.)

Supplemental figure legends

Figure S1. CRISPR screen for regulators of p53 stability.

(A) Flow cytometry blots depicting the dynamic levels of each p53 mutant after x-irradiation (1 Gy) over time.

(B) Unsupervised hierarchy clustering of each screen replicate plotted, visualised as t-distributed stochastic neighbor embedding (t-SNE) blot. The inter-run correlation is computed by comparing the normZ scores of each gene from the two replicates.

Figure S2. CRISPR screen for regulators of p53 stability.

(A-D) Screen results for R175H, G245, R248Q, and R337H p53 stability screen.

(E) Comparison of different p53 mutants and the effects on their stabilities upon perturbation of individual constitutient genes of the proteasomal subunits.

(F) Guides efficiency measured as genetic indel abundances of sgRNAs targeting *CCDC6, FBXO42, and MDM2*, in the clonal RPE1-reporters and PANC1 lines, using Inference of CRISPR Edits (ICE) analysis. The knockout efficiency (indel%) of each guide in the PANC1Cas9 line is displayed as a histogram.

Figure S3. FBXO42-CCDC6 axis regulates p53 stabilities across wild-type and different mutants.

(A) Flow cytometry blots depicting the dynamic levels of indicated p53 mutants to the depletions of CCDC6 and FBXO42 measured 10 days post-transduction.

(B) Flow cytometry blots depicting the dynamic levels of $p53^{R273H}$ mutant to the depletions of CCDC6 and FBXO42 and after x-irradiation (0.5 Gy) over time. The distribution of the population in p53mClover low and high is also displayed.

(C) Western blot analysis of $p53^{R273H}$ protein levels upon depletions of *CCDC6*, or *FBXO42* 10 days post-transduction, and at various time points after irradiation.

(D) Quantification of $p53^{R273H}$ protein levels upon depletions of *CCDC6*, or *FBXO42*, and at various time points after irradiation, measured using flow cytometer at 10 days post-transduction.

The ratios of the bimodal populations (p53-mClover high vs low) from all time points were normalized to the untreated sgAAVS1 control group. (*: $p<0.08$, error bar indicates standard deviation of the mean).

(E) Flow cytometry blots depicting the dynamic levels of $p53^{R273H}$ protein level upon depletion of *CCDC6* or *FBXO42* and treatment with the proteasomal inhibition MG132 (10uM; 12 hours).

(F) Quantitative real-time PCR analysis of the PANC1 cells with depletion of *CCDC6* or *FBXO42*. The *TP53* transcript level was normalised to the house keeping gene Peptidyl-prolyl cis-trans isomerase B (*PPIB*). Experiment performed in biological triplicates.

(G) Western blot showing the expression levels of the FBXO42 full length protein and indicated FBXO42 truncation mutants.

(H) Schematic of FBXO42 and itsfunctional domains to be studied. The Kelch domain numbers correspond to those removed from each subsequent truncation mutant.

(I) Flow cytometry blots depicting the dynamic levels of $p53^{R273H}$ protein levels upon depletion of *FBXO42* and ectopic expression of various FBXO42 truncation mutants measured at 7 days post-transduction. The truncation domains are illustrated by the schematics.

Figure S4. Mapping the genetic interaction network of FBXO42-CCDC6 and mutant p53.

(A) Interaction of CCDC6 and p53R273H in PANC1 cells validated using immunoprecipitation (IP). Lysates of PANC1 cells overexpressing V5-tagged CCDC6 or a EGFP control construct with or without genetic ablation of the endogenous $p53^{R273H}$ gene were immunoprecipitated using an V5-specific antibody, followed by Western blot analysis of endogenous p53.

(B) Flow cytometry blots depicting the dynamic levels of $p53^{R273H}$ protein level upon depletion of *CCDC6* or *FBXO42* or *USP28* or concomitant depletion of *USP28* and *CCDC6* or concomitant depletion of *USP28* and *FBXO42*.

(C) Immunofluorescence imaging showing localization and levels of $p53^{R273H}$ (FITC) and USP28 (Alexa 568) in RPE1 R273H reporter cell lines with control or clonal depletion of *CCDC6* or *FBXO42*.

(D) Quantitative real-time PCR analysis of the PANC1 cells with depletion of *CCDC6* or *FBXO42*. The *USP28* transcript level was normalised to *PPIB*. Experiment performed in biological triplicates.

(D) Flow cytometry blots depicting $p53^{R273H}$ levels upon ectopic expression of *CCDC6* or *FBXO42*, measured at 7 days post-transduction.

(E) Flow cytometry blots depicting $p53^{R273H}$ levels in R273H-reporters with clonal depletions of USP28 (left), FBXO42 (middle) or CCDC6 (right), upon ectopic expression of *CCDC6 FBXO42* or *USP28*, measured at 7 days post-transduction.

Figure S5. C16orf72 functions as oncogene and regulates p53 stability in the mammary gland

(A) Flow cytometry blots depicting the levels of p53 G245S, R248Q, and R248W in the reporters upon depletion of *C16orf72*.

(B) cBioPortal OncoPrint displaying mutations of *C16orf72* found in all cancers.

(C) cBioPortal OncoPrint displaying a trend toward co-amplification between *USP7* and *C16orf72* in all cancers.

(D) cBioPortal OncoPrint displaying a trend toward mutual exclusivity between genetic ablation of *TP53* and *C16orf72* amplification, and co-amplification between *USP7* and *C16orf72*, among breast cancer patients.

(E) Kaplan-Meier plot comparing the tumour-free survival of tumour-prone mouse line (LSL-$Pi3k^{H1047R}$) with loss of Trp53 (sgTrp53-Cre) or control (sgTigre-Cre), delivered via mammary ductal injection of lentiviruses carrying each ORF. (n=5 for each condition.)

Materials and methods

Materials Availability

DNA constructs and other research reagents generated by the authors will be distributed upon request to other academic research investigators under a Material Transfer Agreement. In addition, DNA constructs will also be deposited to Addgene.

Cell lines

RPE1-hTERT (ATCC CRL-4000) and PANC-1 (ATCC CRL-1469) cell lines were maintained in Dulbecco's modifed Eagle's medium (DMEM; Wisent Inc.), supplemented with 10% (vol/vol) fetal bovine serum (Wisent Inc.), 100 U/ml of penicillin, and 100 mg/ml of streptomycin (Wisent Inc.) at 37°C under 5% CO_2.

To generate RPE1-based clonal stability reporters, RPE1-hTERT-Cas9-TP53-KO cells [75] were transduced with recombinant pLKO.1-based lentiviruses carrying the p53mClover-P2A-mRFP1 cassette at 0.1 MOI, and single clones selected. The pLKO.1-based p53mClover-P2A-mRFP1 cassette carrying control (no p53), wild-type, or hotspot mutant p53s was generated by restriction enzyme cloning, where all hotspot mutants were first generated using site-directed mutagenesis in the pDONR223 entry clone vector and then sub-cloned into the cassette.

To further generate clonal reporters depleted of hit genes, the RPE1-based reporter was transfected with CRISPR ribonucleoprotein (RNP) complexes containing Cas9 and guides against the gene-of-interests. Clonal lines were selected and verified for homozygous deletions by both PCR-based Inference of CRISPR Edits (ICE) and Western blotting.

To generate other cell lines stably expressing Cas9, each line was transduced with lentiviruses expressing lentiCas9-Blast (Addgene #52962) and selected by Blasticidin to generate either single or clonal lines as specified.

CRISPR and FACS based screens

Stability reporters (150 million (M) cells total) cultured on 15 cm dishes (3 M/plate) were first transduced with the lentivirus-based Toronto Knockout v3 library (TKOv3) [37] at a low MOI (~0.30). They were then puromycin-selected [17 μg/mL] for two days for transductants starting at 24th hour-post-transduction (hpt). At 48 hpt, cells were trypsinized and replated back to the same plates while maintaining puromycin-selection. At 72 hpt (time point T0), remaining cells were pooled together, counted to confirm MOI, and divided into two technical replicates (referred to as p53.1 and p53.2 in figures) for subculturing; 30 M cells were further collected to confirm the library gRNA abundance at T0. The subcultured replicates were further maintained in puromycin-free media and passaged every three days (T3 and T6).

10 dpt (T7), all cells were harvested by trypsinization and subjected to live sorting by Fluorescence-Activated Cell Sorting (FACS). Harvested cells were resuspended in FACS sorting buffer (Hanks Balanced Salt Solution, 25 mM HEPES pH 7.0, 2 mM EDTA, 1% Fetal Bovine Serum) at a concentration of 5 M cells per mL and were filtered by 40 μm nylon mesh to eliminate large aggregates. All cells were then live-sorted based on both the mClover and mRFP1 signals, where only populations with medium-mRFP1 signals were collected to eliminate populations with large gene-expression changes. For mutants displaying bi-modal-mClover populations, all cells from the mClover-low and mClover-high were individually collected; for uni-modal mutants, cells with mClover intensity within the highest and lowest 15% population were individually collected. (Fig. 1d) Both technical duplicates were independently sorted and collectively maintained the 200X coverage.

Upon sorting, gDNA from cell pellets was isolated using Wizard Genomic DNA Purification Kit (Promega, Cat# A1120); genome-integrated sgRNA sequences were then amplified by PCR using Q5 Mastermix Next Ultra II (New England Biolabs, Cat# M5044L), with primers v2.1-F1-5' GAGGGCCTATTTCCCATGATTC 3' and v2.1-R1-5' GTTGCGAAAAAGAACGTTCACGG 3', followed by a second round of PCR reaction containing i5 and i7 multiplexing barcodes. Final PCR products were gel-purified and sequenced on Illumina NextSeq500 systems to determine sgRNA representation in each sample.

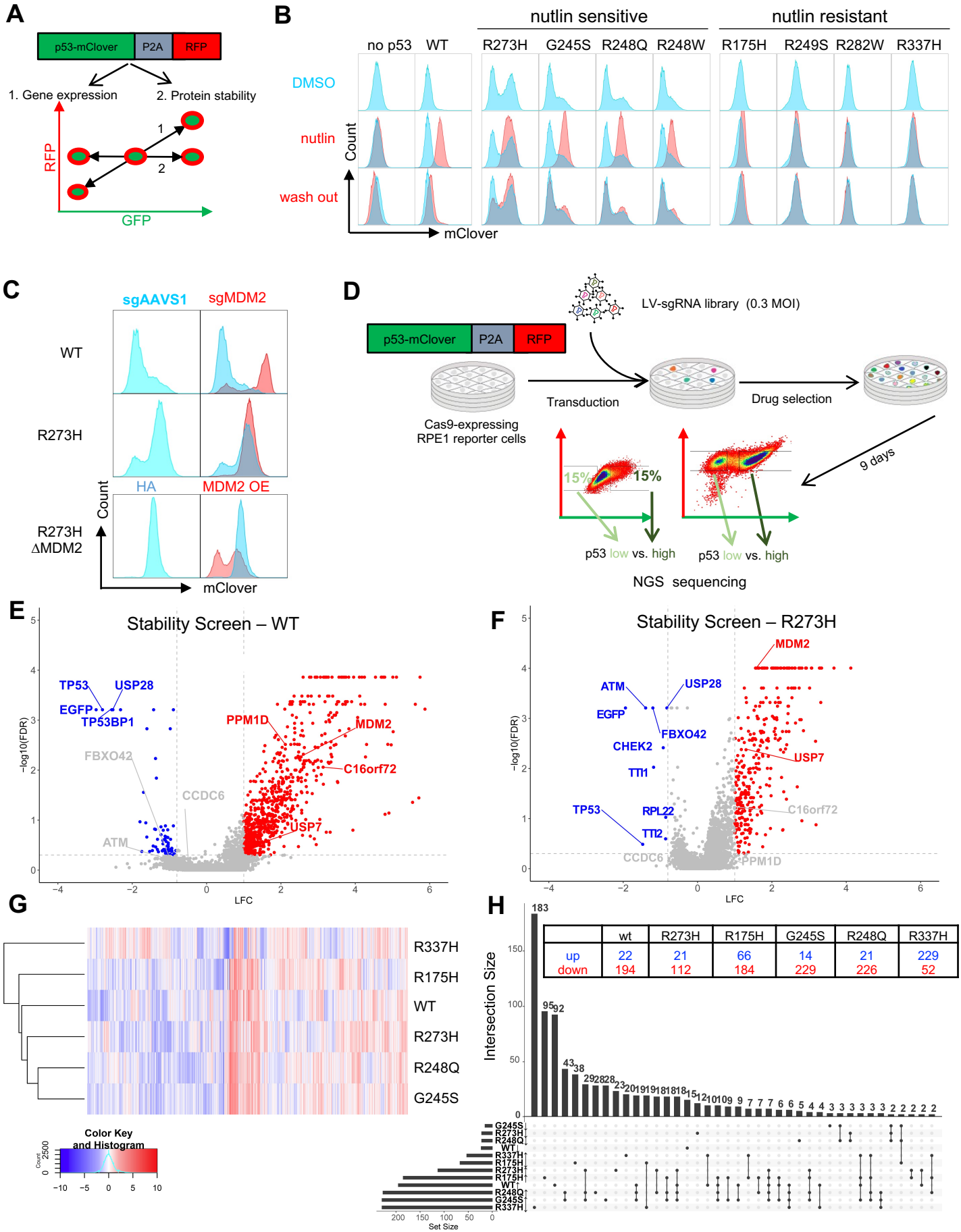

	wt	R273H	R175H	G245S	R248Q	R337H
up	22	21	66	14	21	229
down	194	112	184	229	226	52

Figure 1. CRISPR screen for regulators of p53 stability.

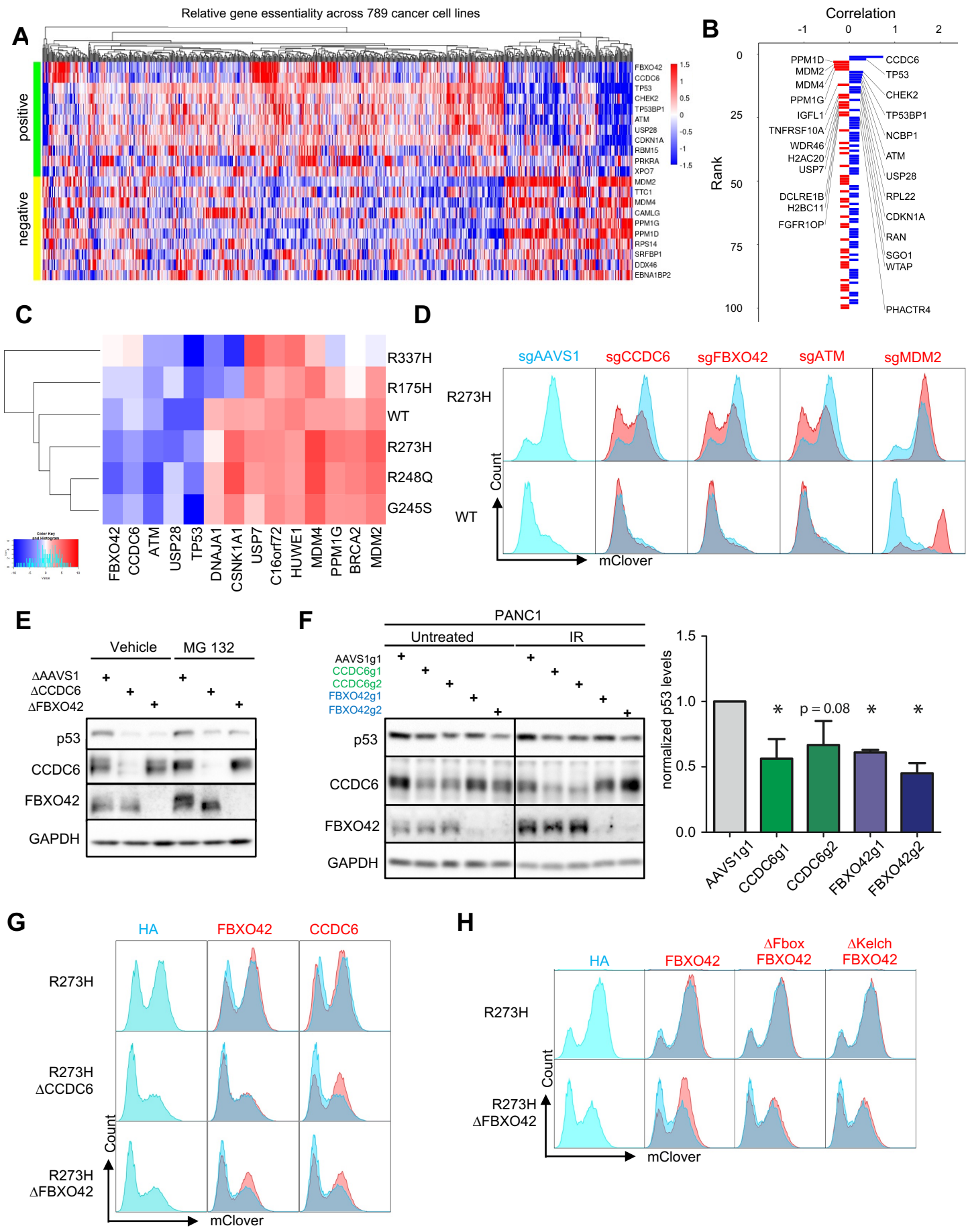

Figure 2. FBXO42-CCDC6 axis regulates mutant p53 protein stability

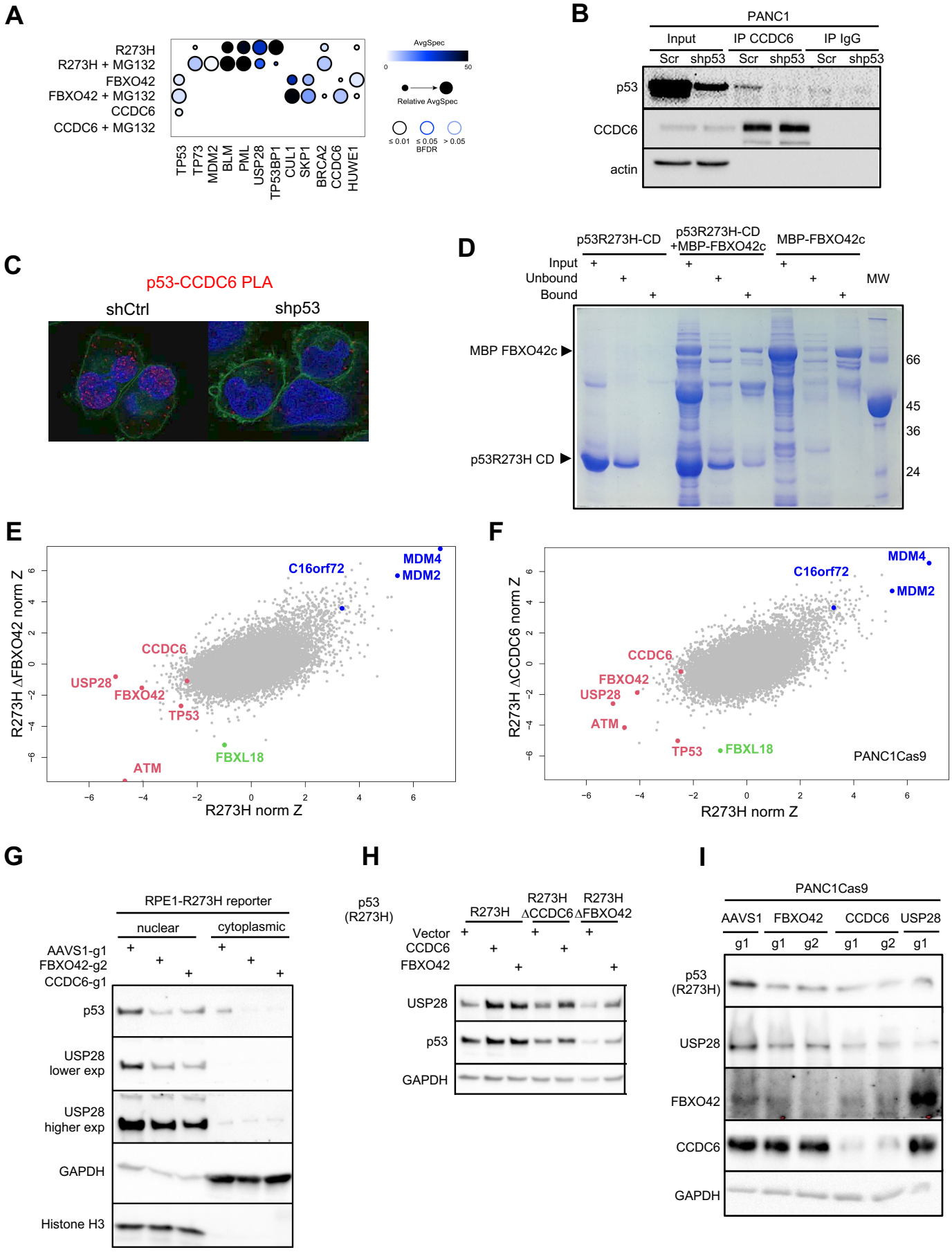

Figure 3. Mapping genetic interactions of FBXO42-CCDC6-R273H

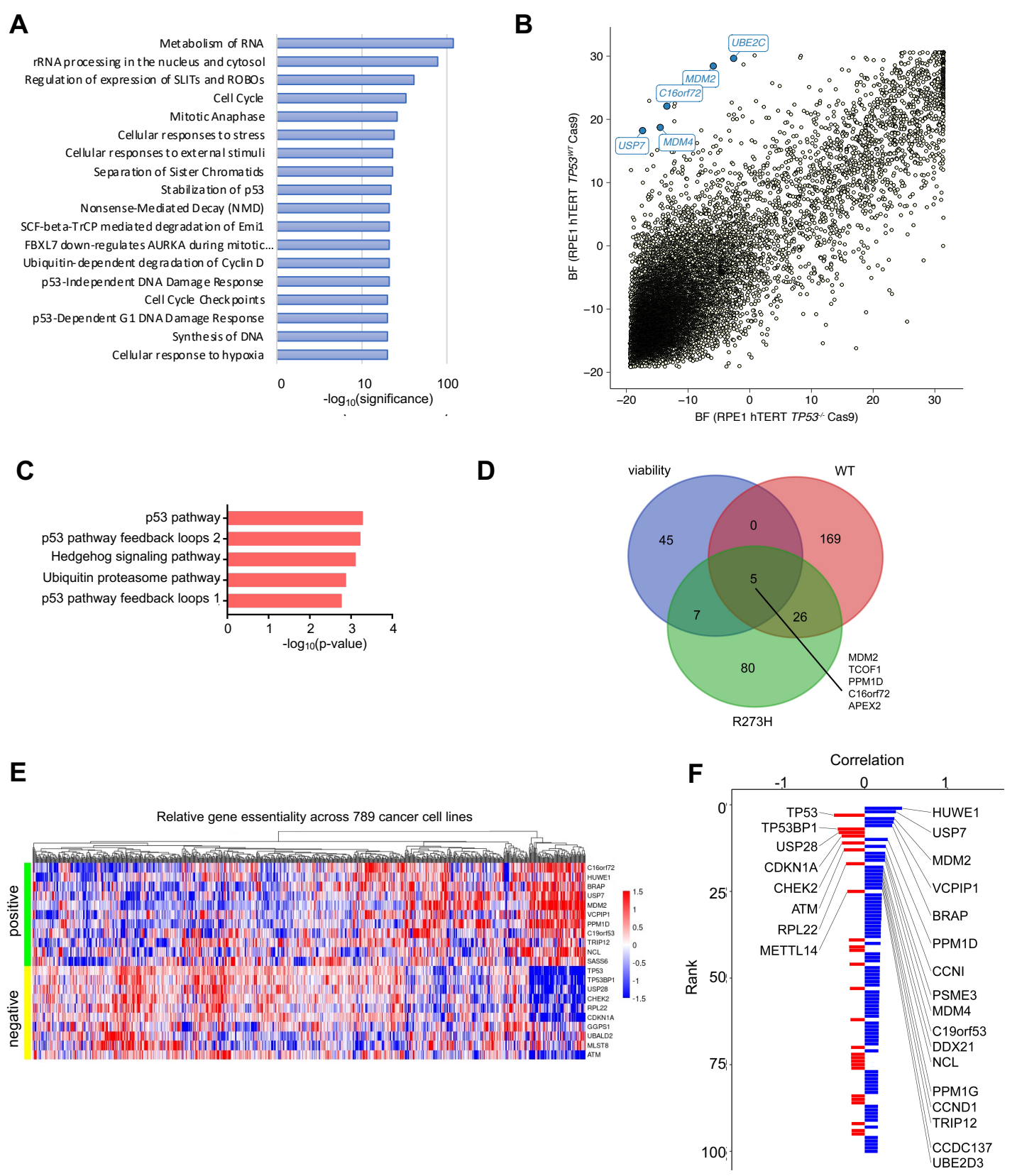

Figure 4. Synthetic viability screen maps regulators of p53

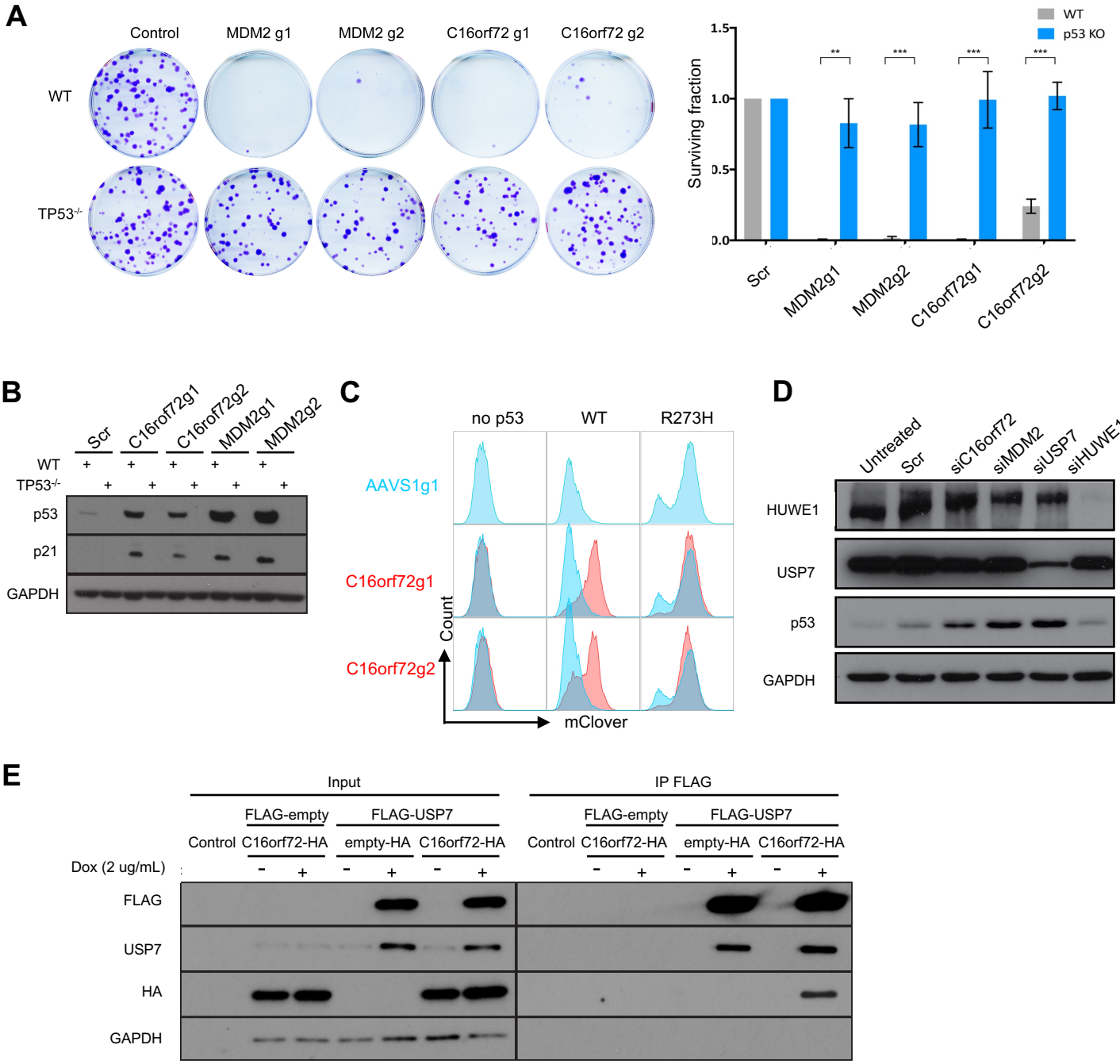

Figure 5. C16orf72 is a regulator of wildtype and mutant p53 stability.

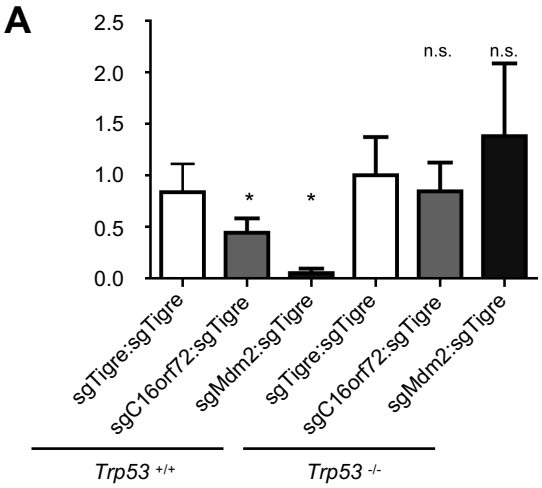

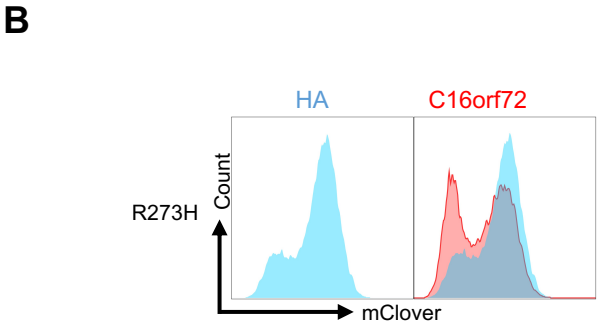

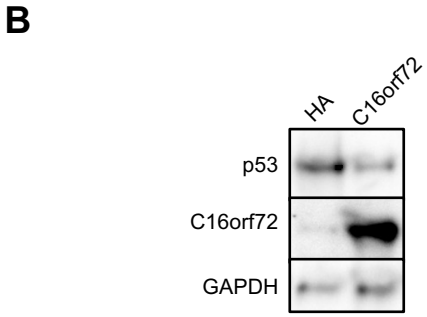

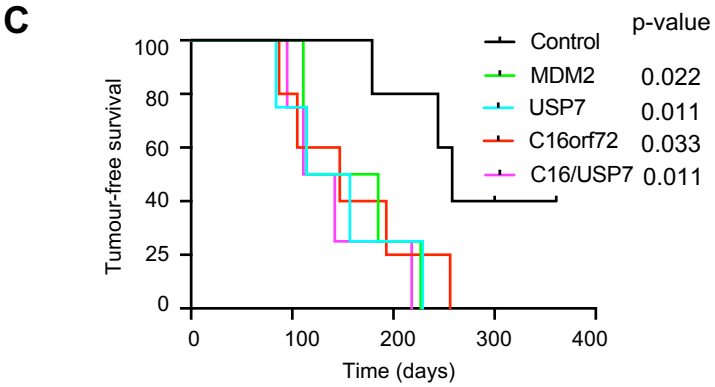

Figure 6. C16ORF72 functions as oncogene and regulates p53 stability in the mammary gland.